Local and Remote Responses to Excessive Snow Mass over Eurasia Appearing in the Northern Spring and Summer Climate —A Study with the MRI·GCM—

By Tetsuzo Yasunari

Institute of Geoscience, University of Tsukuba, Tsukuba, Ibaraki 305, Japan

and

Akio Kitoh and Tatsushi Tokioka

Meteorological Research Institute, Tsukuba, Ibaraki 305, Japan
(Manuscript received 7 September 1990, in revised form 11 June 1991)

Abstract

The effect of excessive snow mass over the Eurasian continent on the spring and summer climate is investigated by using the MRI·GCM. The ensemble mean of the four runs (SNOW runs) with the excessive snow mass of 5 cm (water equivalent) at the beginning of March over the snow cover area of the continent is compared with that of the control runs, to deduce the effect of the snow mass on the climatic parameters in the later seasons.

The main results are summarized as follows:

(1) In spring, the albedo effect is dominated in the lower latitudes particularly over the Tibetan Plateau. The reduced net radiation by the anomalous snow cover balances the reduced surface sensible and latent heat fluxes, which account for the significant decrease of surface temperature, cloudiness and total diabatic heating over there in the SNOW runs.

(2) In summer, in contrast, the snow-hydrological effect is significant, particularly in the mid-latitudes. The increase of ground wetness in the SNOW runs causes anomalous cooling and higher pressure near the surface. A moderate signal of the weakened Asian summer monsoon is also obtained. However, the increase of evaporation activates cumulus convection, which partly compensates for the decrease of total diabatic heating by the cooling near the surface. This evaporation/convection feedback seems to work, on the other hand, to sustain the increased ground wetness throughout the summer.

(3) The atmospheric teleconnection patterns induced by the anomalous snow cover over the Tibetan Plateau and east Asia significantly appear over the north Pacific and the North American continent in spring through late summer. These anomalous circulations cause the considerable decrease of surface temperature over the northeastern part of North America.

(4) The implication of these results for the Ice Age issue is also briefly discussed.

1. Introduction

At the end of the last century, Blanford (1884) first pointed out the possible relationship between the Himalayan spring snow cover and the succeeding summer monsoon rainfall over India, though his result attracted little attention from meteorologists for a long time afterwards. By using satellite snow cover data over Eurasia, Hahn and Shukla (1976) re-demonstrated the link, showing the apparent reverse relationship between the Eurasian snow cover extent in winter and the India monsoon rainfall in the following summer. Several succeeding studies (Dey and Bhanu Kumar, 1983: Dickson, 1984, *etc.*) confirmed their results.

In addition, recent observational studies have strongly suggested that the snow cover over Eurasia plays an important role in producing the anomalous condition of the coupled ocean/atmosphere system in the equatorial Pacific (*e.g.*, El Niño) by means of the Asian monsoon (Barnett, 1985; Yasunari, 1987, 1990, 1991).

These observational relationships between the Eurasian snow cover in winter and spring and the tropical climate system in later seasons are sug-

gested to be based principally on two physical processes. One is the albedo effect, as suggested by Hahn and Shukla (1976). The high albedo of the snow reduces the total incoming solar radiation, which may in turn reduce the heating of the ground surface of the continent from spring to summer season. Some general circulation model (GCM) studies with the Ice Age surface boundary conditions (Williams, 1975; Manabe and Hahn, 1977; Prell and Kutzbach, 1988, *etc.*) have supported this idea.

The other process is the snow-hydrological effect, which was first examined by Yeh *et al.* (1983) by using a simplified GCM. Miyakoda and Chao (1982) pointed out the importance of this effect on long-range forecasting. Recently, Barnett *et al.* (1989) attempted to discuss this effect as well as the albedo effect more comprehensively by the aid of GCM experiments with full physics and geography. That is, the snow mass not only consumes the solar energy during the snow melting, but also reduces the heating of the ground after the snowmelt by moistening the surface soil layer with the melted snow. This effect may provide a plausible explanation of the time-lag relation between the winter snow cover and the summer monsoon. Yamazaki (1989) has suggested that the combination of these two effects is actually important for producing the anomalous atmospheric condition over the continent in summer. These two effects of snow cover are schematically shown in Fig. 1.

On the other hand, recent observational studies have suggested some significant time-lagged teleconnection patterns in the mid-latitudes induced by the anomalous snow cover over Eurasia. By using lag-correlation synoptics Morinaga (1987) and Morinaga and Yasunari (1987) deduced some significant lag-correlation patterns between the anomalous snow cover over central Asia and the atmospheric anomalies, particularly on the downstream-side of the continent. Kodera and Chiba (1989) showed that the Okhotsk high intensity at 500 mb in June, which is an important factor in controlling the Baiu (frontal rain) activity over Japan, is highly correlated to the snow cover anomaly over central Asia in April, presumably by means of stationary wave trains over eastern Eurasia. Iwasaki (1991) pointed out the apparent 1-year lag correlation between the snow cover over eastern Eurasia and that over the north American continent.

Furthermore, Kuhle (1987) argued the possibility of the "Tibetan Ice Sheet" during the Quaternary Ice Age and its role on triggering the global-scale glaciation itself.

The results of these observational and paleoclimatic studies urge us to assess more quantitatively the effects of the Eurasian snow cover anomaly on the local as well as remote or global-scale responses under different basic states of atmosphere.

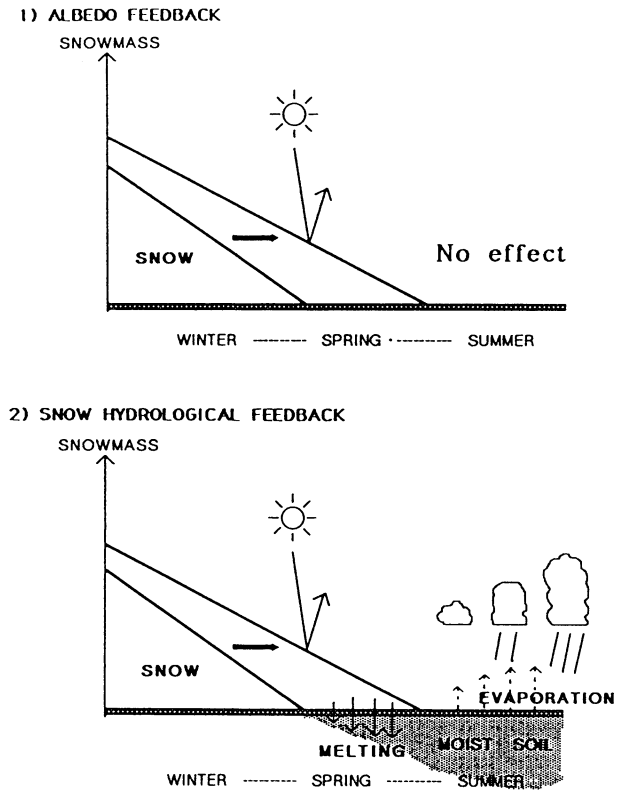

Fig. 1. Schematic diagram for the albedo feedback and the hydrological feedback of snow cover during the seasonal march from winter to summer.

For example, it has not been clear how and to what extent the snow mass anomalies of each season and each area produce atmospheric circulation anomalies via the anomalous energy balance on the ground surface and in the atmosphere. Seasonal as well as spatial dependencies seem to be crucial for the two physical processes (Fig. 1). Particularly, the relative importance of snow cover anomalies over the Tibetan Plateau should be investigated in more detail from these points of view. How the snow cover process interacts with other physical processes, *e.g.*, ground-hydrology, evaporation and cumulus convection, may also be a key factor for producing atmospheric anomalies.

This study focuses on these problems through the analysis of the GCM experiments with anomalous snow cover in spring over Eurasia.

2. Design of GCM experiments

2.1 The Model

The GCM utilized for this study is a tropospheric version of the MRI·GCM-I (Tokioka *et al.*, 1984) produced at the Meteorological Research Institute (MRI). The model atmosphere consists of 5-layers in the vertical with a top at 100 mb, and has a horizontal grid resolution of 5° in longitude and 4° in latitude. The formulation of diabatic processes includes

the cumulus parameterization of Arakawa and Schubert (1974), interacting with the planetary boundary layer (PBL) and the radiative process. The diurnal and seasonal variations of solar insolation are taken into account.

The land surface processes in the model are as follows: The soil moisture is predicted by using the one-layer bucket model with a field capacity of 15 g cm^{-2}. The heat and water budgets at the model surface are governed by

$$CdT_g/dt = R_s - R_L - F_s - F_w + H_i, \tag{1}$$

$$dW/dt = P_r - E - R + S_m, \tag{2}$$

$$E = \beta E_p, \tag{3}$$

$$\beta = \min(1.0,\ 2 \times GW), \tag{4}$$

$$GW = W/W_{\max}, \tag{5}$$

$$R = \left(R_r^3 + D_w^3\right)^{1/3} - D_w, \tag{6}$$

$$D_w = W_{\max} - W, \tag{7}$$

T_g is the ground temperature, C the bulk heat capacity of the ground, R_s the solar flux absorbed at the surface, R_L the net upward longwave flux at the surface, F_s the sensible heat flux, F_w the latent heat flux (*i.e.*, $F_w = L \times E$, L is the latent heat of water vapor), H_i the snow melt and/or heat conduction through sea ice, W the available soil moisture, P_r the precipitation rate, E the evapotranspiration rate, R the surface runoff, S_m the snowmelt, the evapotranspiration efficiency, E_p the potential evapotranspiration rate, GW the ground wetness, $W_{\max}$ the maximum available soil moisture, and D_w the soil moisture deficiency. Here, $W_{\max} = 15$ g cm^{-2} is adopted for all land grid points. Surface runoff R is a function of P_r and D_w (see Eq. (6)), so that it can occur when rainfall occurs even if the ground is not saturated.

The seasonally varying land surface albedo is adopted from Matthews (1983) depending upon vegetation conditions. Surface albedo over the ocean is taken from Posey and Clapp (1963). Surface albedo (α) over the snow is a function of snow mass and masking depth of snow which depends on the terrain height as follows:

$$\alpha = \begin{cases} \alpha_b + (\alpha_s - \alpha_b)\sqrt{\dfrac{S_N}{d_{sw}}} & S_N < d_{sw} \\ \alpha_s & S_N \geq d_{sw} \end{cases} \tag{8}$$

where α_b is the bare land albedo by Mathews (1983), α_s is the deep snow albedo ($=0.70$), S_N is the snow mass. The masking depth of snow d_{sw} is defined as follows:

$$d_{sw} = \max(1, 5 - 2h)$$

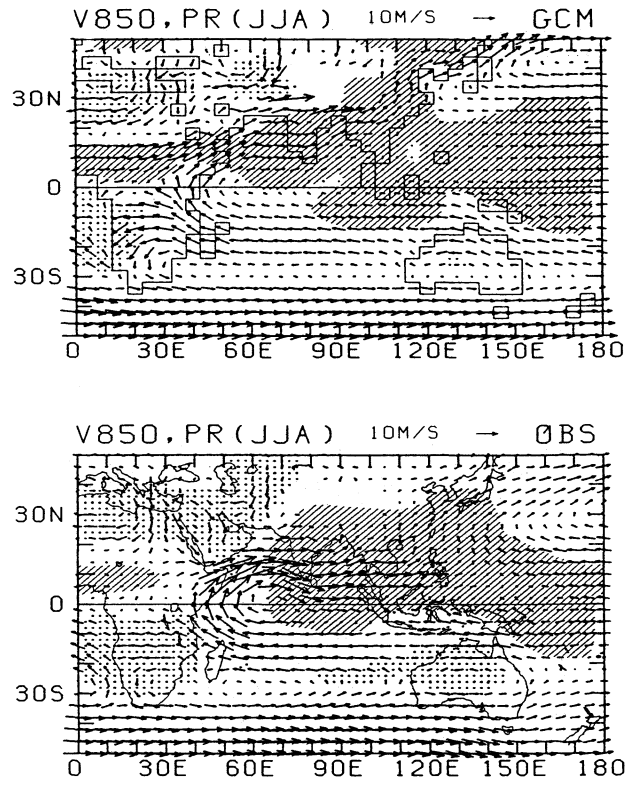

Fig. 2. (Upper) simulated precipitation and wind vector at 850 mb in the control run for the northern summer. The shaded (dotted) area denotes precipitation of more than 5 mm (less than 1 mm) per day. (Lower) observations based on the 1979–87 NMC wind and the Jaeger (1976) precipitation.

where h is the surface terrain height in km.

The sea surface temperature is prescribed with the monthly climatological data over the whole ocean. The snowfall rate is predicted by using the precipitation rate and the air temperature at the surface. The snow mass over land is predicted as a result of heat balance of the land surface.

2.2 Experiments

The model is integrated for three and a half years starting from March 1 as a control run (hereafter referred to as the CNTL run). The model performance of the CNTL run, particularly for the Asian monsoon is essential as a premise of the evaluation of the anomaly run discussed later. This CNTL run is fundamentally the same as Kitoh and Tokioka (1986) and Kitoh *et al.* (1988), which successfully reproduced the Asian and African monsoons. Fig. 2 shows the mean wind vector field at 850 mb and total precipitation for summer (June, July, August) from (a) the CNTL run and (b) the observations. The large-scale features of the Asian monsoon, such as the southwest monsoon flow over the Arabian sea,

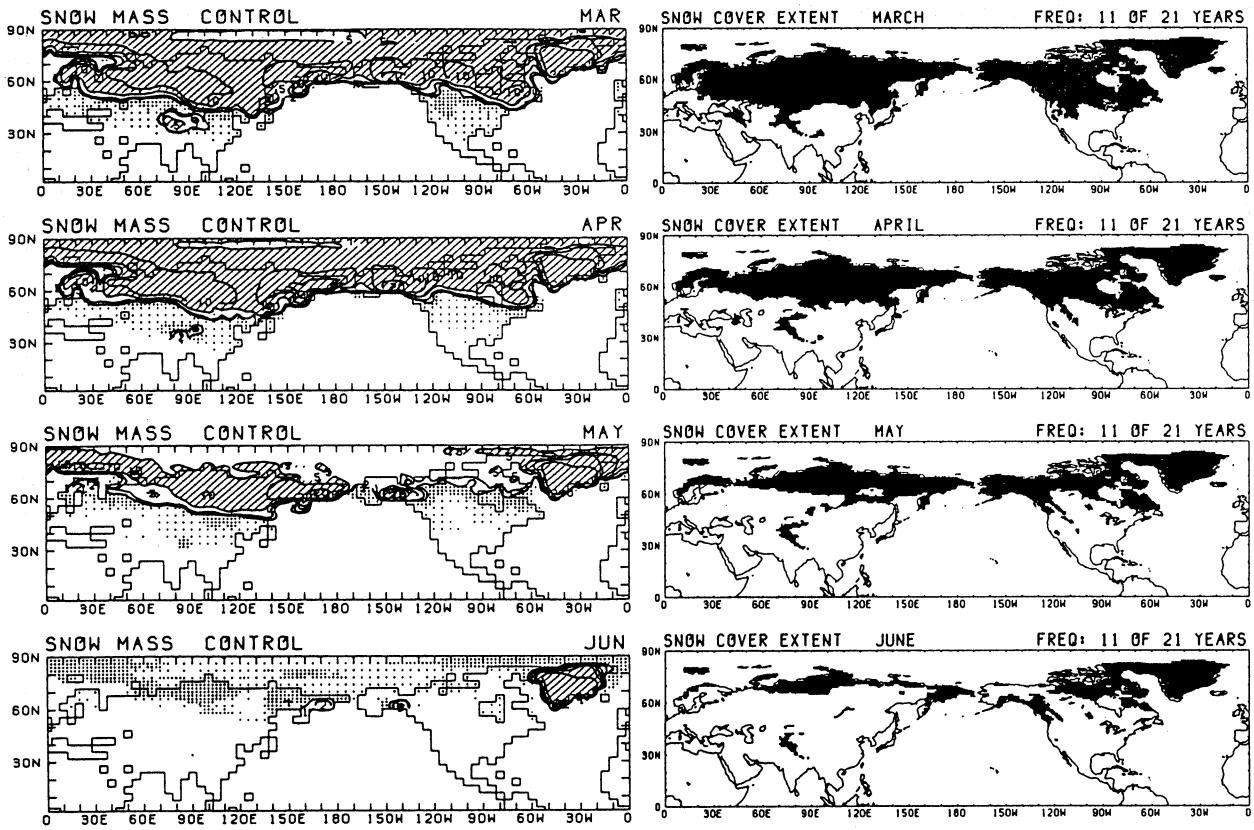

Fig. 3. Snow mass distribution in the CNTL run (left) and observed snow cover extent from NOAA/NESDIS data (right) for March through June. In the left diagrams, values of more than 1.0 cm (water equivalent depth) are shown with solid lines, and values of more than 5 cm are shaded. Values between 1.0 cm and 0.1 cm are heavily dotted. and those between 0.1 cm and 0 cm are lightly dotted. In the right diagrams, snow cover frequency of more than 50 % (during the 21 years) are indicated.

rainfall distribution over the monsoon Asia and central Asia, subtropical high over the Pacific *etc.*, are simulated well in the CNTL run, though the rainfall and westerly wind over the equatorial western Pacific is considerably less than the observations.

In the anomalous snow cover run (hereafter referred to as the SNOW run), 5 cm (water equivalent) snow mass anomaly was added only over the snow-covered area between 30°N and 60°N of the Eurasian continent on March 1 of every CNTL run year as an initial condition to minimize the shock of abrupt change in the integration. The model is integrated for 184 days up to September 1. Maximum snow mass in the CNTL run appeared at the end of February, which is nearly coincident with that of the observation. A remarkable feature in the CNTL run is a very reasonably simulated seasonal change of snow cover area if we refer to the observation from NOAA/NESDIS data, as shown in Fig. 3. Although the best climatology of (water equivalent) snow depth over Eurasia is not yet available, the maximum snow depth distribution in the CNTL run seems to be highly compatible with the observed distribution from Schutz and Bregman (1987) over the major part of the continent. The snow depth in the model tends to show a larger value locally in the lower latitudes and in the eastern part of the continent.

Four half-year (March to August) sets of the SNOW run are thus obtained as shown in Fig. 4, and the ensemble means of the outputs from the four SNOW runs are compared with those from the four corresponding CNTL runs, to deduce the effects of the anomalous snow cover in spring (March 1). It may be a tough question as to how reasonably we can give the snow mass anomaly in the model, since we have so far very little information about the interannual as well as seasonal variability of real snow mass (depth) on the continental scale. However, recent satellite-derived snow depth information from Nimbus-7 SMMR data for 7 years (Chao *et al.*, 1987) suggested the areal-mean year to year maximum snow depth over the whole snow-covered area ranges 5 cm to 8 cm (water equivalent), which implies that a 5 cm (water equivalent) anomaly over the major part of Eurasia seems to be a very reasonable value for the interannual variability in the present climate. The mean snow mass distribution in the CNTL run and the anomaly added in the SNOW run on March 1 are shown in Fig. 5.

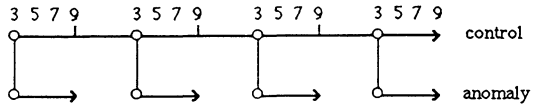

Fig. 4. Design of the GCM experiment for the control (CNTL) runs and the anomaly (SNOW) runs.

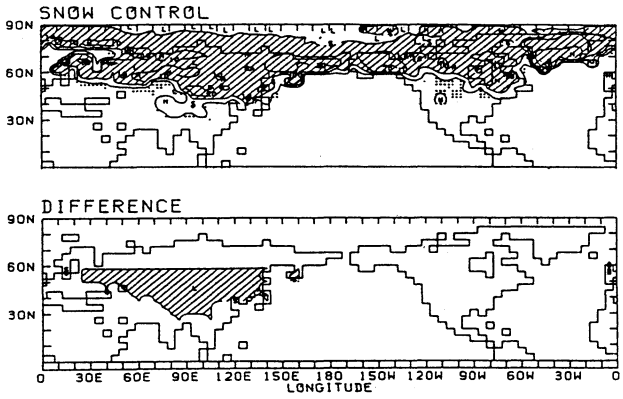

Fig. 5. Distribution of anomalous snow cover (5 cm water equiv alent depth) added in the SNOW run on March 1.

3. Changes in the suface condition over Eurasia

Since the two physical processes, *i.e.*, the albedo effect and the snow-hydrological effect, are supposed to be essential for producing the anomalies in the atmosphere as shown in Fig. 1, the differences in surface parameters over the Eurasian continent between the CNTL run and the SNOW run are examined in this section. Figure 6 shows the seasonal change (from March to August) of the monthly mean values of the two runs and the anomaly (SNOW run–CNTL run) of snow mass and albedo averaged over the Eurasian continent east of 75°E. The increases of albedo in the SNOW run are noticeable along the southern periphery of snow cover area of each month in spring (March to May), mostly corresponding to the delayed snowmelt. This albedo change is, however,, hardly recognizable after June, when the snow-covered area over Eurasia almost completely disappeared in the SNOW as well as the CNTL runs.

Figure 7 shows the same diagram as Fig. 6 but for surface air temperature (T_s) and soil moisture (GW). The T_s (and GW) anomaly shows totally negative (and positive) values particularly in the mid-latitudes (30°N–50°N), undoubtedly associated with the excesses in snowmass and albedo (Fig. 6). It should be noted that there seem to be two stages in the seasonal march of the negative Ts anomaly, one in the lower latitude (around 30°N) in spring (March and April), and the other in the higher lat-

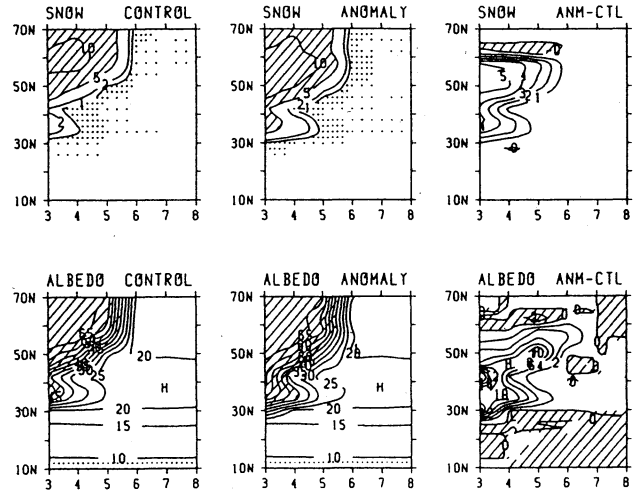

Fig. 6. Seasonal change (from March to August) of monthly mean snow mass (upper) and albedo (lower) of each latitude for the CNTL run (left), SNOW run (middle) and its difference (SNOW-CNTL) (right). The unit of snow mass is cm (water equivalent). The heavily (lightly) dotted area in snow mass shows 0.1–1.0 (0–0.1) cm depth. The unit of albedo is %. Areas of 5 cm (40 %) or larger are shaded in snow mass (albdo) diagrams of CNTL and SNOW runs. Negative values are shaded in the SNOW-CNTL diagrams.

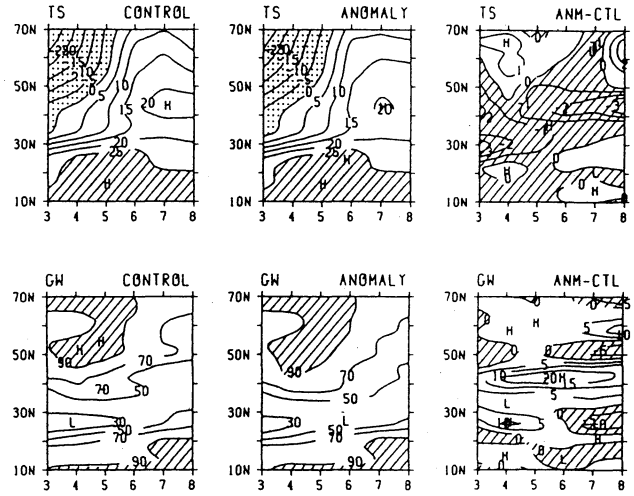

Fig. 7. Same as Fig. 6 but for surface air temperature (TS) and ground wetness (GW). The unit of TS is C. The unit of GW is % of the full water storage (15 cm water equivalent).

itudes (40°N–50°N) in summer (June to August). A similar feature in the positive GW anomaly is also noted, but in this case the anomaly in the second stage (in summer) is far larger than that in the first stage (in spring).

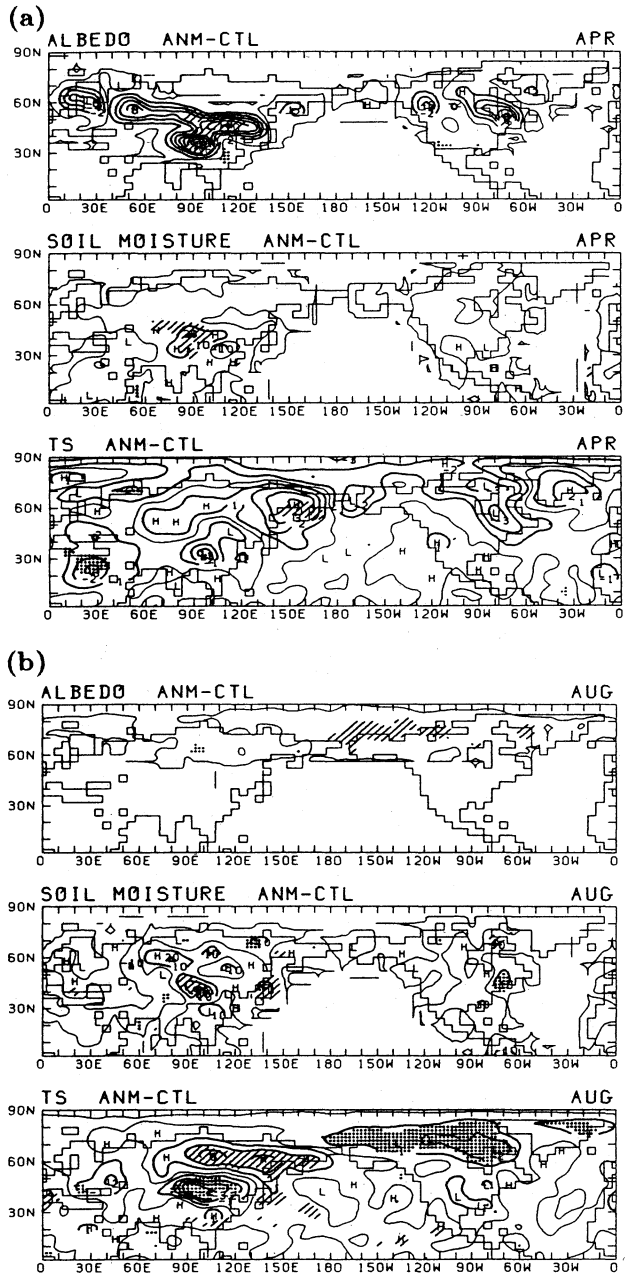

Fig. 8. Distributions of albedo (%), GW (%) and Ts (°C) anomalies over the northern hemisphere in (a) April and (B) August. Areas of positive (negative) anomaly with the significant level of 5 % or less are shaded (dotted).

The distributions of albedo, GW and T_s anomalies over the northern hemisphere in April and August are shown in Fig. 8, to see more precisely the difference in the spatial distribution of these anomalies between spring and summer. It is apparent that the negative T_s anomaly as well as the positive albedo and GW anomaly in the subtropics (30°N) in spring (April) are mostly due to the significant anomalies over the Tibetan Plateau. In summer (August), on the other hand, the large negative T_s anomaly in mid-latitudes (40°N–50°N) is mostly related to the anomaly in east Asia to the northeast of the Tibetan Plateau.

The distribution of the GW anomaly is complicated, but the area of the large negative Ts anomaly between 80°E and 120°E totally corresponds to the positive GW anomaly there. However, there is no albedo anomaly there. It is worthwhile to state that the large anomalies in the second stage (over east Asia in summer) appear completely after the snowmelt over the whole of Eurasia while those in the first stage (over the Tibetan Plateau in spring) seem to be related to the in-situ snowmass and albedo anomaly. These features suggest that the effect of snow cover appears in a different way depending upon seasonal timing and geographical location, as is also pointed out by Barnett *et al.* (1989). This aspect will be discussed further in the next section.

4. Changes in heat and water balance over Eurasia

The large negative Ts anomalies at the two stages (*i.e.*, in spring and in summer) are supposed to result from the different physical processes at the surface, since the anomalies of other related parameters (GW, albedo, *etc.*) have shown considerably different features between the two stages. To examine this aspect more in detail, the seasonal changes of heat and water balance at the surface and in the troposphere, and their anomalies (SNOW run–CNTL run) are computed for the typical areas at each stage, that is, over the Tibetan Plateau (32°N–40°N, 75°N–105°E), and over east Asia (40°N–48°N, 90°E–120°E), as shown in Fig. 9 and Table 1, respectively.

Over the Tibetan Plateau in April (the first stage) the albedo effect is dominant as shown in Table 1. This stage is obviously characterized by the fact that snow exists where normally it would not. In the SNOW run the net short-wave radiation (RS) is significantly reduced due to the large positive snowmass (SN) or albedo (α) anomaly. Because of the relatively cooled surface, both latent heat flux (FW) and sensible heat flux (FS) are considerably suppressed. Less cloudiness (N) and precipitation (Pr) associated with more stable atmosphere and relatively downward motion may be responsible for the significant reduction of total heating (Q) in the atmospheric column.

Over east Asia in August (the second stage), in contrast, although there is no SN and α anomaly, large negative Ts and Tg anomalies are still apparent. This is due to the relative cooling of the surface basically by the increase of FW (evaporation) and the decrease of FS, which are directly related to the increase of GW after the snowmelt of the excessive snowmass. In addition, less RS due to the increase of cloud cover (N) through the increased evaporation

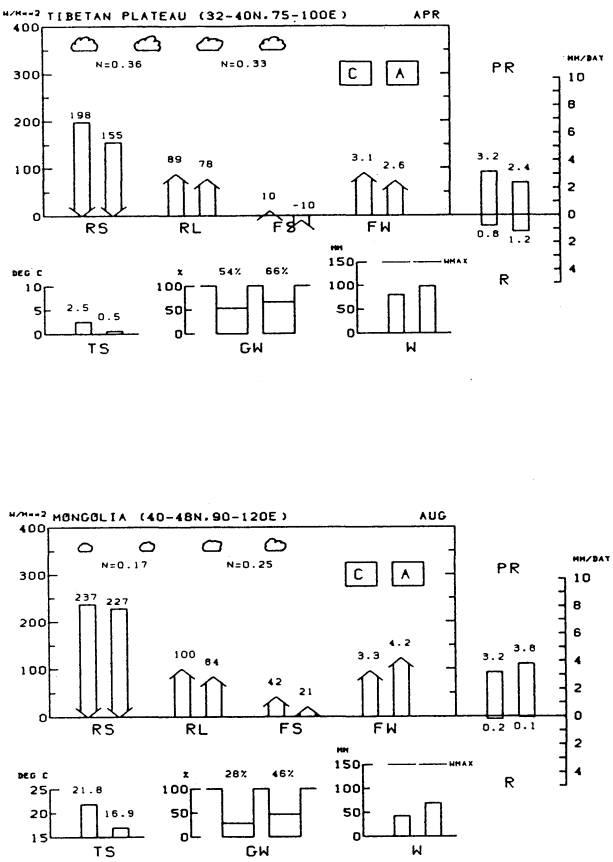

Fig. 9. Surface heat and water balance and cloudiness over (a) Tibetan Plateau in April and (b) east Asia in August. The left (right) column of each pair represents the value in the CNTL (SNOW) run. Units and notations are indicated in Table 1.

may also be partly responsible for the large negative Ts (or Tg) anomaly. This snow-hydrological effect on Ts (and Tg) becomes more significant in late summer (July and August) than in early summer (June), presumably because evaporation nonlinearly increases as Ts (or Tg) increases following Clausius-Clapeyron's law.

Although the decrease in Ts and Tg is extremely large in the SNOW run, there is no significant change in Q, which implies that the increased diabatic heating in the upper and middle part of the troposphere by cumulus convection, caused by the increased evaporation from the surface compensates the cooling effect near the surface. The increased Pr, on the other hand, has a role in the maintenance of wet ground throughout the summer. That is, the snow-hydrological effect in this model seems to be very effective for cooling in the lower troposphere, but not for the reduction of total heating in the whole troposphere. This characteristic nature of the model response to the excess snowmass and wet ground seems to be closely associated with the cumulus parameterization of Arakawa and Schubert (1974), where cumulus convection is very sensitive to evaporation, or more directly, the moisture amount in the planetary boundary layer (PBL).

5. Asian summer monsoon anomalies

The anomalies in some Asian summer monsoon indices, induced by the excess snow mass in the SNOW run are described here. As is pointed out in the previous section, the snow-hydrological effect in this model to the total heating of the atmosphere is more or less diluted by the evaporation/cumulus convection feedback. Nevertheless, some signals of a weakened Asian summer monsoon are found, particularly in late summer (July and August). Sea level pressure (SLP) over the continent is a measure of land surface heating. Figure 10 shows the monthly mean SLP in the CNTL run and the anomaly (SNOW run—CNTL run) for August. There is an indication of a weaker monsoon trough over northern India (positive SLP anomaly) in the SNOW run, although it is not significant. It is interesting to note that a large negative SLP anomaly area is seen along the northern and eastern periphery of the positive SLP anomaly, and another broad area of positive anomaly exists over Alaska and the north polar region. These significant anomalies are discussed further below.

The other parameters particularly related to the monsoon activity (*i.e.*, wind, precipitation, diabatic heating, divergence) show the weakening of the monsoon in the SNOW run, though most of the anomalies are marginally significant. Figure 11 shows the same diagram as Fig. 10 but for the wind field at 850 mb. The easterly anomaly over the Arabian sea is noticeable, indicating the weaker southwest monsoon flow in the SNOW run. This weaker monsoon wind is consistent with the weaker monsoon trough over northern India.

Another important measure of the monsoon is precipitation. Figure 12 shows the same diagram as Fig. 10 but for the total precipitation. The CNTL run has simulated well the broad feature of the observed distribution of Asian summer monsoon rainfall (*e.g.*, refer to Legates (1987)). The anomaly distribution shows a general decrease of rainfall of about 20 % in the area of maximum monsoon rainfall over southeast Asia. Over northeast Asia and central Asia, in contrast, a positive anomaly of precipitation is noticeable, associated with the snow-hydrological feeadback as discussed in Section 4.

The total heating of the atmosphere over India through southeast Asia is also considerably reduced. Associated with the reduced atmospheric heating and convective rainfall, the velocity potential field in the upper troposphere (200 mb) shows a weakened divergent monsoon circulation over south and southeast Asia, as shown in Fig. 13. Although this weakened monsoon circulation in the SNOW run is

Table 1. Anomaly (SNOW run–CNTL run) of heat and water budget over (a)the Tibetan Plateau and (b) Mongolia (east Asia). Gothic values are those with the significant level of 5 % or less.

Heat and Water Budget

a) Tibetan Plateau (32–40N, 75–105E)

mon	SN	$1-\alpha$	RS	RL	FW	FS	HG	N	Ts	Tg	Q	E	R	Pr	GW
Mar	**5.2**	**−9**	**−25**	**−12**	−5	**−9**	0	**7**	**−0.9**	−0.3	−6	−0.2	0.0	0.3	0.3
Apr	**3.5**	**−14**	**−43**	−11	−17	**−20**	**5**	−3	−1.9	−3.1	**−52**	−0.6	0.0	**−0.8**	**1.8**
May	0.0	−4	−15	−5	5	−19	**4**	**−3**	−1.5	−2.3	**−33**	0.2	0.0	−0.4	2.0
Jun	0.0	−0	−5	−4	3	−4	1	3	−0.8	−0.7	−4	0.1	0.0	0.0	1.1
Jul	0.0	−0	−6	−5	6	−6	−0	**5**	−0.7	−0.2	7	0.2	0.0	0.4	1.1
Aug	—	—	−1	1	−0	−1	−0	1	−0.1	−0.1	1	−0.0	0.0	−0.0	0.9

b) Mongolia (40–48N, 90–120E)

mon	SN	$1-\alpha$	RS	RL	FW	FS	HG	N	Ts	Tg	Q	E	R	Pr	GW
Mar	**4.6**	**−15**	**−26**	**−9**	**−12**	**−4**	−1	3	**−2.6**	**−3.3**	**−21**	**−0.4**	0.0	−0.4	0.5
Apr	2.4	**−9**	−20	−7	−12	−7	**6**	3	−0.8	−1.3	−6	−0.4	**0.1**	0.2	**2.1**
May	0.4	−3	−15	−8	−5	−7	4	6	**−2.0**	**−1.9**	4	−0.2	0.1	0.3	**2.6**
Jun	0	−0	−7	**−8**	**18**	**−17**	0	4	**−2.4**	**−1.8**	−0	**0.6**	0.0	0.5	**3.2**
Jul	—	—	−4	**−13**	**32**	**−24**	0	4	**−3.6**	**−2.7**	12	**1.1**	−0.0	**1.3**	**2.6**
Aug	—	—	**−10**	**−16**	**27**	**−21**	0	**8**	**−5.0**	**−3.2**	−5	**0.9**	−0.0	0.6	2.7

SN	snow depth (cm water)	Ts	surface air temperature (°C)
$1-\alpha$	1 − surface albedo (%)	Tg	ground temperature (°C)
RS	net shortwave radiation (W/m^2)	Q	total diabatic heating (W/m^2)
RL	net longwave radiation (W/m^2)	E	evaporation (mm/d)
FW	latent heat flux (W/m^2) = L × E	R	runoff (mm/d)
FS	sensible heat flux (W/m^2)	Pr	precipitation (mm/d)
HG	net heat budget at the surface	GW	soil moisture (cm water)
N	cloudiness (%)		

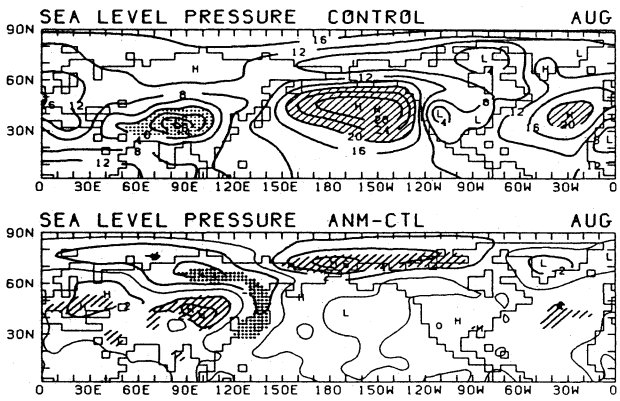

Fig. 10. Monthly mean SLP in the CNTL run (upper) and the anomaly (SNOW run–CNTL run) for August. In the upper diagram, pressure values of 1020 mb or more (1000 mb or less) are shaded (dotted). In the lower diagram, positive (negative) values with the significant level of 5 % or less are shaded (dotted).

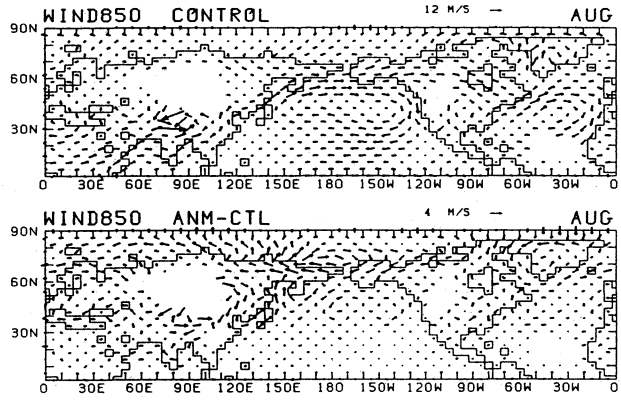

Fig. 11. Same as Fig. 10 but for wind vectors at 850 mb.

typically shown in August, similar features associated with the weakened convective activity over the southeast Asia through the western Pacific are also apparent during late spring (May) through summer. Thus, the weakening of the Asian summer monsoon

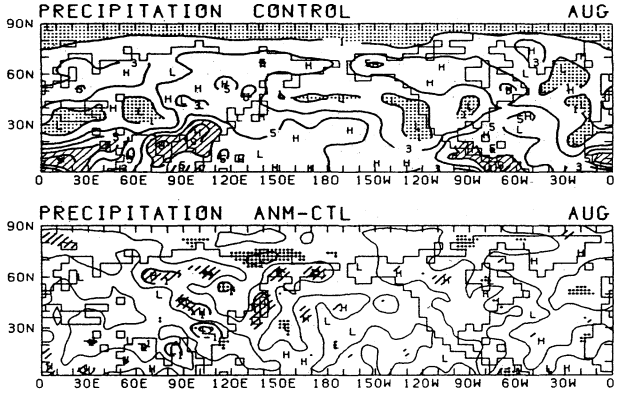

Fig. 12. Same as Fig. 10 but for precipitation. In the upper diagram, values of 7 mmday^{-1} or more (1 mm day-1or less) are shaded (dotted). In the lower diagram, positive (negative) values with the significant level of 5 % or less are shaded (dotted).

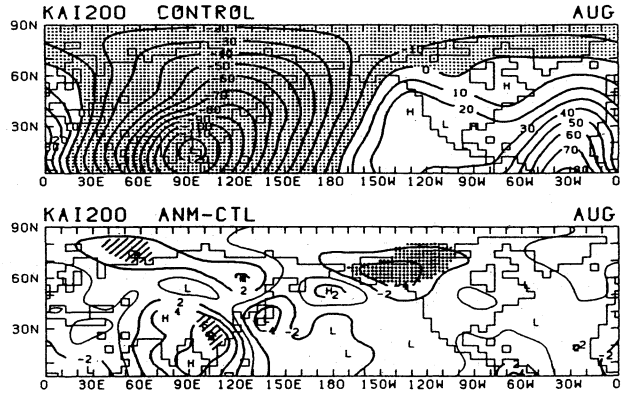

Fig. 13. Same as Fig. 10 but for velocity potential at 200 mb.

principally by the snow-hydrological effect of the anomalous snowmass has been confirmed. These results for the Asian summer monsoon, are fundamentally the same as obtained by Barnett *et al.* (1989), though the details of the experimental procedures and the results are quite different from each other. Further comparisons between the present results and theirs will be made later.

6. Teleconnections in middle and high latitudes

It has been established both from observations and theories (Hoskins and Karoly, 1981; Webster, 1982 *etc.*) that the anomalous diabatic heating induced by the anomalous surface heating condition produces anomalous local and remote responses in the atmospheric circulation field. Some observational studies have suggested that the anomalous snow cover over Eurasia induces the in-situ and remote anomalous circulation referred to in the introduction. Here the anomalous circulation field (SNOW runs—CNTL runs) is examined from this point of view.

Figure 14 shows the monthly mean geopotential height anomaly at 500 mb from March to August. In spring the anomalous patterns are very similar to each other, particularly in March and April. A negative anomaly is significant over east Asia. It should be noted that to the northeast of this negative anomaly there exist a distinct positive anomaly area over Kamchatka Peninsula/far east Siberia and also another negative anomaly over the Labrador/Baffin Bay area, suggesting the propagation of a Rossby wave train forced by the anomalous vorticity over east Asia. The negative height anomaly over east Asia can be explained as a local response to the increased diabatic cooling over and around the Tibetan Plateau (see Table 1 and Fig. 8) and the increase of diabatic heating over the north Pacific near the east coast of Asia, as theoretically pointed out by Smagorinsky (1953). Interestingly, the same type of anomaly pattern was obtained in the observed anomaly pattern for April, relevant to the anomalous snow cover over central Asia (Morinaga, 1987).

In June an area of large negative anomaly appears over the Kamchatka Peninsula where the Okhotsk high is located in this season. An area of positive anomaly is also found over the Canadian arctic region, to the northeast of the negative anomaly, and another area of negative anomaly is marked over the northeast of North America, which again shows a Rossby wave-train pattern originated from the Okhotsk high area.

The change of the anomaly pattern over east Asia from the previous spring months may be related to the change of the seasonal basic state there. The monthly mean total heating field shows that in this month the heating/cooling contrast between the continent and the ocean is completely reversed from the winter and spring condition to the early summer condition, *i.e.*, heating over the continent and cooling over the Okhotsk sea. This seasonal change in horizontal contrast of diabatic heating seems to be essential for the formation of the Okhotsk high or ridge in the middle troposphere (Asakura, 1968). The anomalous cooling over the continent by the snow-hydrological effect weakens the heating contrast, and may result in the weakening of the Okhotsk high or ridge. Surprisingly enough, the anomaly pattern shown here is quite similar to that deduced from the observed lag-correlation pattern between the anomalous snow cover over central Asia in April and 500 mb height anomaly in June (Kodera and Chiba, 1989), as reproduced here in Fig. 15.

In July there is no significant change in the circulation patterns as a whole. This seems to be related to the basic state of the zonal wind and the spatial

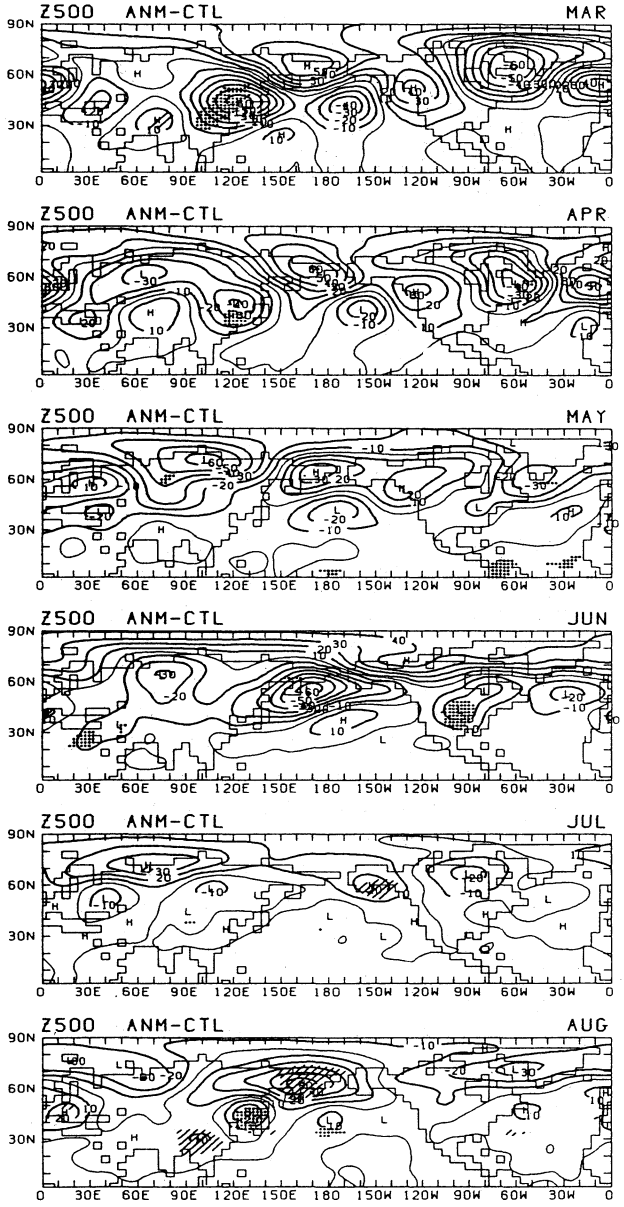

Fig. 14. Monthly mean geopotential height anomaly at 500 mb in March through August. Positive (negative) values with the significant level of 5 % or less are shaded (dotted).

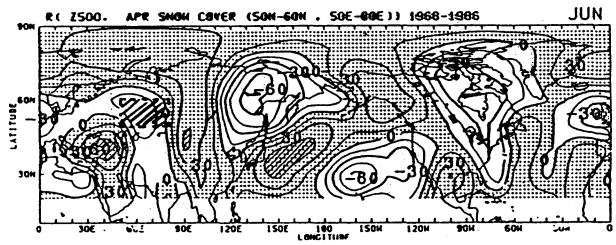

Fig. 15. Correlation coefficients ($\times 100$) between April snow cover over central Asia (50°–80°E, 50°–60°N) and 500 mb height in June, based on the data for 1968–86. Positive values (of 0.45 or more) are dotted (shaded). (Kodera and Chiba, 1989).

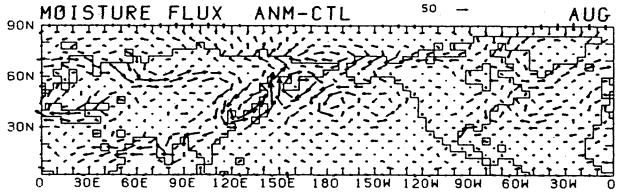

Fig. 16. Moisture flux anomaly (SNOW run–CNTL run) at 850 mb in August. The unit is g m s^{-1}.

distribution of total heating in this month. The mid-latitude westerly wind in this month over Eurasia is the weakest in the year, and the area of maximum heating associated with the Asian monsoon is confined to the easterly zone in the lower latitudes both in the CNTL run and the SNOW run. Under this condition the anomalous cooling near the surface by the anomalous soil moisture in east Asia seems to be too small to produce effectively the anomalous circulation in the mid/high latitudes.

In August the anomalous circulation with the Rossby-wave-like pattern is again evolved over east Asia through the arctic north American region. A remarkable feature in this month is the anomalous heat source and upper-level divergence (Fig. 13) over the coastal area of east Asia, *i.e.*, over Japan islands. This anomalous heat source seems to be related to the activated baroclinic disturbances associated with the intensified warm and moist advection from the southeast ahead of the intensified trough there, as shown in Fig. 16. It is noteworthy that this intensified trough seems to have been non-linearly amplified by the interaction of cold air advection along the north-eastern periphery of the anomalous cold high in the lower troposphere over the Mongolian region and the warm air along the east coast of the Eurasian continent, as is demonstrated in Fig. 10 and Fig. 11. The mean westerly wind in the troposphere over this region has become stronger than that in July, which enables a stronger teleconnection on the downstream side.

Barnett *et al.* (1989) also noted the teleconnection patterns over east Asia through the north American continent in their model results for the anomalous snow cover over Eurasia, though the spatial scales of their anomaly patterns are generally far larger than those of ours. This difference between the two model results may be due to the difference of the spatial scales as well as the thickness of snow cover anomaly given in each model. The snow mass anomaly in their model seems to have a whole-continent scale, while that in our model is more regionally confined

to the interior of the continent. This aspect of the snow cover issue, *i.e.*, the sensitivity of the teleconnection pattern to the size and volume of snow cover anomaly, may be one of the important problems to be investigated further.

7. Discussion

7.1 Seasonality in the snow feedbacks

The aforementioned results have elucidated that the feedback of anomalous snowcover over the Eurasian continent produces atmospheric anomalies through the anomalies in the surface heat and water balance. The albedo effect is proved to be significant in spring in the lower latitude, particularly over the Tibetan Plateau, where the incoming solar radiation in this season is extemely strong. Although the direct response of the atmosphere (*e.g.*, lower Ts, higher SLP *etc.*) to this effect is limited over and around the Tibetan Plateau, the indirect response by way of the teleconnection appeared nearly hemispherically as described in Section 6. This result at least partly contrasts with the argument by Barnett *et al.* (1989).

During summer months, the snow-hydrological feedback has induced a weakening of the Asian summer monsoon to some extent, particularly in the SLP, precipitation and divergence field. The anomalies of these parameters over the monsoon region are, however, generally less significant and more localized in size than those appearing in the experiments by Barnett *et al.* (1989). This may be partly due to the enormous snow mass anomaly in their experiments, where the snow mass difference between their SNOW (D) run and the CNTL (C) run in June averaged over Asia was 10 cm. In our experiments this difference in June was only traceable over the limited area of northern Asia, as shown in Fig. 6, which seems to be more realistic if we compare the seasonal change of our model snow mass distribution to that of the observed snow mass distribution estimated from Nimbus-7 SMMR data (Morinaga and Igarashi, 1991).

7.2 Evaporation/convection feedback

Another reason for a less significant monsoon in our SNOW runs may be due, as commented in Section 4, to stronger evaporation/cumulus convection feedback in our model. That is, the areas of positive soil moisture anomaly in the SNOW run correspond well with the areas of positive anomaly in evaporation, water vapor content in the PBL, precipitation, and total diabatic heating in the air column particularly in summer months (not shown). This effect may at least partly dilute the cooling effect of evaporation near the surface to the total heating of the atmosphere, by adding the more cumulus heating in the middle and the upper atmosphere.

This result contrasts with that by Barnett *et al.* (1989), where surface cooled by surplus moisture flux suppresses convection there. This notable difference between the two model results may be partly due to the difference of cumulus parameterization in the models. In our model with the Arakawa-Schubert scheme, convection seems to be more sensitive to the moisture amount in the PBL than their scheme (*i.e.*, Kuo's parameterization), where it needs large-scale moisture convergence.

On the other hand, this evaporation/convection feedback enhances and prolongs the snow-hydrological feedback near the surface by increasing cloudiness and precipitation, which tend to sustain reduced Rs and increased GW and, as a result, lower Ts and higher SLP throughout the summer. Fundamentally the same results as ours are noted in the GCM experiment by Yeh *et al.* (1984), who examined the effect of the excessive soil moisture on the climate anomaly. They pointed out that the excessive soil moisture over the mid-latitude rain belt tends to prolong the moisture anomaly and increase precipitation by recycling water between land surface and atmosphere. By contrast, this effect is relatively weak over the dry regions in the subtropics.

We have so far very little information about the real feature of cumulus convection and precipitation in the interior of the Eurasian continent in summer. We should emphasize, however, that this evaporation/convection feedback is supposed to be feasible particularly over the seasonally-heated continent in summer, where large-scale convergence in the lower troposphere is generally dominant. In fact, the GCM experiment by Delworth and Manabe (1989) with the realistic geography also suggests that this feedback by soil moisture anomaly is significantly large in the middle latitudes over the continent in summer. Once this feedback works over east Asia through the interior of the continent in the mid-latitudes, localized circulation anomalies may be produced there by the anomalous diabatic heating in the middle and upper troposphere.

It seems to be crucial for the snow-hydrological feedback, therefore, how the increased evaporation by the excessive snow affects convection/precipitation processes. In other words, the characteristic nature of the combined snow-hydrology /evaporation/convection feedback seems to provide a clue for the late effect of snowmass to the summer climate. This may really be a new but important aspect of the snow cover issue that should be examined further. It includes the assessment of, *e.g.*, the large-scale water cycle, and of a more realistic cumulus parametarization over the interior of the summer continent, associated the snow-hydrological process during spring through summer.

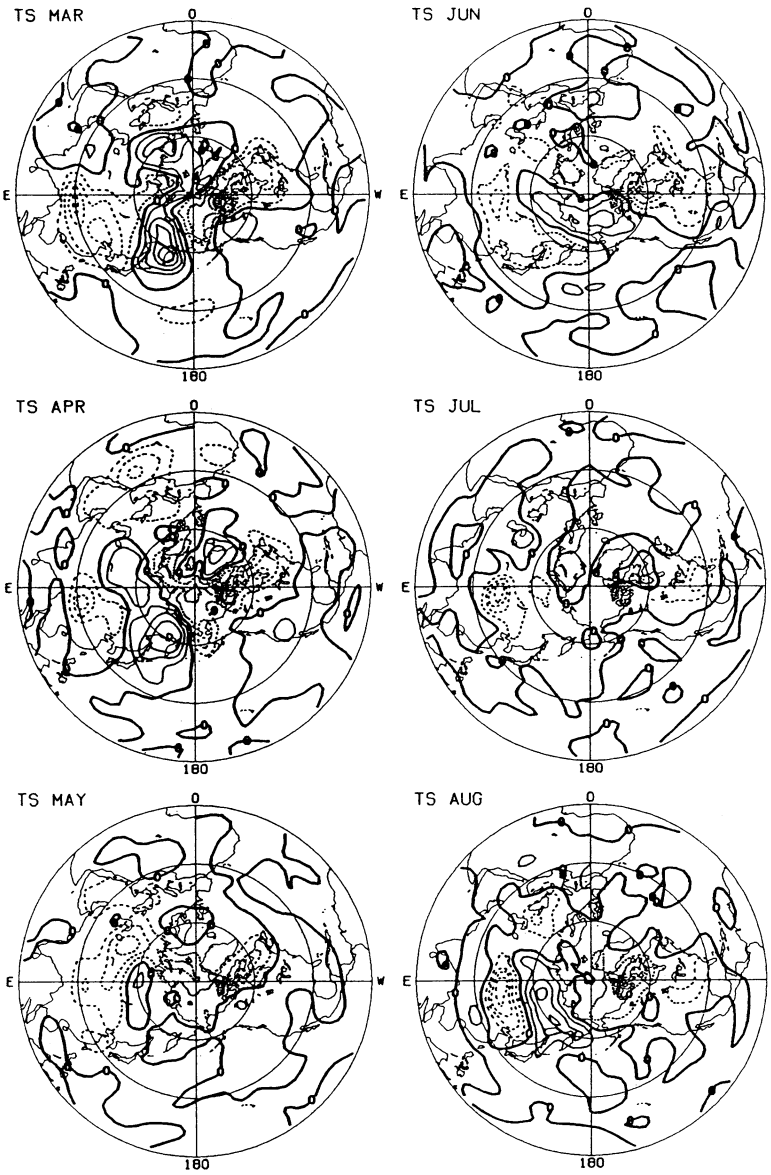

Fig. 17. Surface air temperature anomaly in March through August. Contours are 1°C and negative values are dashed.

7.3 Teleconnection over North America and the Ice Age issue

The PNA-like teleconnection pattern during spring through summer, induced by the anomalous forcing over east Asia associated with the anomalous snow mass over Eurasia, may be one of the important features of the general circulation in this experiment. This model result is in good agreement with the observed circulation pattern deduced by Kodera and Chiba (1989) (Fig. 15). Yasunari (1988) has also offered observational evidence for the dominance of this pattern particularly in late summer of a weak Indian monsoon year. Large month to month changes in the teleconnection patterns may be most probably due to the seasonal changes of the zonal mean state, as has been noted by Kang (1990).

Associated with this pattern, an intense anomalous trough at 500 mb over the northeast part of the North American continent (Fig. 14) has appeared during spring through summer in the SNOW run. This persistent trough may be very important for the issue of the Ice Age initiation, since this trough seems to provide a favorable condition (*i.e.*, persistent negative Ts anomaly) for the snow accumulation there, as shown in Fig. 17. We will note here the important implication of the present result for the Ice Age problem.

Lamb (1977), for example, suggested that the formation of an ice sheet over the North American continent could lead the earth to the stage of full glaciation by triggering another ice sheet over Scandinavia by way of the downstream adjustment of stationary planetary waves. He commented further that the persistent cold trough over this region even

through the warmer seasons may be a key factor for the formation of the Laurentide Ice Sheet, though he did not mention how the cold trough could have been maintained. Kuhle (1987) suggested, on the other hand, the key role of the cooled Eurasian continent, particularly the completely-glaciated Tibetan Plateau, in triggering hemispheric cooling and glaciation, though he did not mention the possible dynamical process of hemispheric cooling.

The present result may suggest a common answer to their questions. That is to say, the persistent anomalous snow cover over Eurasia including the Tibetan Plateau, which might be the first signal of reduced solar radiation by some external or internal forcing, could be responsible for the anomalous circulation over North America noted by Lamb (1977), by means of the downstream teleconnection deduced here. In fact, a very recent model study by Short *et al.* (1991) has suggested that the maximum response of surface temperature change associated with the Milankovitch forcing occurs over the interior of the Eurasian continent, not over the polar regions. A recent GCM study by Oglesby (1990) also showed that in addition to Alaska, western Canada and Siberia, the Tibetan Plateau is one of the "glaciation sensitive" regions to the initial imposition of heavy snow cover. These problems should, of course, be further examined by the long-term integration of the models with interactive oceans.

8. Conclusions

The effect of excessive snow mass over the Eurasian continent on the spring and summer climate has been investigated by performing the MRI ·GCM model experiments. The ensemble mean of four SNOW runs with the excessive snow mass of 5 cm (water equivalent) on March 1 over the snow cover area of the continent has been compared with that of the CNTL runs, to deduce the effect of the snow mass on the climatic parameters. The main results are summarized as follows:

(1) In spring, the albedo effect is dominated in the lower latitudes particularly over the Tibetan Plateau. The reduced net radiation by the anomalous snow cover balances the reduced surface sensible and latent heat fluxes. Cloudiness is also reduced and the total diabatic heating in the atmosphere is considerably diminished. Although the direct response of the atmosphere to this effect is more or less localized, the teleconnection pattern induced by this localized anomaly seems to be an important feature of the total influence of the snow cover.

(2) In summer, the snow-hydrological effect is significant particularly in the mid-latitudes. The increase of ground wetness in the SNOW run causes anomalous cooling and higher pressure near the surface. However, the change in the total diabatic heating is not significant mainly due to the evaporation/cumulus convection feedback, which partly counteracts the cooling near the surface. This evaporation/convection feedback seems to work, on the other hand, to sustain the increased ground wetness throughout the summer.

(3) Some parameters of the Asian summer monsoon activity indicate a weaker monsoon in the SNOW run, although the snow-hydrological effect seems to have been diluted to some degree by the evaporation/convection feedback as mentioned above. Associated with this weak monsoon signal, the sea level pressures have increased over the Asian monsoon region through the equatorial Indian Ocean as a whole in early northern summer. This feature is consistent with the observed initial stage of an ENSO event.

(4) A remarkable feature in this experiment is the atmospheric teleconnection patterns over the north Pacific through the North American continent, induced by the anomalous snow cover over the Tibetan Plateau and east Asia during spring through late summer. These circulation patterns are responsible for the considerable decrease of surface temperature particularly over the northeastern part of North America. These results are partly supported by the observed circulation anomalies associated with the weak Asian monsoon condition (Yasunari, 1988). The signatures in this experiment also suggest the possible role of the anomalous snow cover over Eurasia on the initiation of the Ice Age.

The results obtained here are, however, still tentative since the parameterization of ground hydrology, which may be a key factor of the snow-hydrological feedback, is too simple in this model. The interaction of snow-hydrology feedback with the evaporation/cumulus convection feedback may also be an important problem to be further investigated for this snow cover/climate issue. The remote responses related to the ENSO and the Ice Age issues may be very interesting aspects of the Eurasian snow cover, but these problems should be re-examined by the more sophisticated coupled atmosphere/ocean GCMs.

Acknowledgements

This work was done as a co-opearative study between the Institute of Geoscience, University of Tsukuba and the Meteorological Research Institute. It was also partly supported by the Grant-in-Aid for Scientific Research by the Ministry of Education, Science and Culture No. 01460055. The authors would like to thank Dr. T. Barnett for his critical comments, which substantially improved the paper.

References

Arakawa A. and W.H. Schubert, 1974: Interaction of a cumulus cloud ensemble with the large-scale environment. Part I. *J. Atmos. Sci.*, **31**, 674–701.

Asakura, T., 1968: Dynamic climatology of atmospheric circulation over east Asia centered in Japan. *Papers Meteor. Geophys.*, **19**, 1–68.

Barnett, T.P., 1985: Variations in near-global sea level pres sure. *J. Atmos. Sci.*, **42**, 478–501.

Barnett, T.P., L. Dümenil, U. Schlese, E. Roeckner and M. Latif, 1989: The effect of Eurasian snow cover on regional and global climate variations. *J. Atmos. Sci.*, **46**, 661–685.

Blanford, H.F., 1884: On the connexion of Himalayan snowfall and seasons of drought in India. *Proc. Royal Soc. London*, **37**, 3–22.

Chao, B.F., W.P. O'Conner, A.T.C. Chang, D.K. Hall and J.L. Foster, 1987: Snow load effect on the earth's rotation and gravitational field, 1979–1985. *J. Geophys. Res.*, **92**, B9, 9415–9422.

Delworth, T. and S. Manabe, 1989: The influence of soil wetness on near-surface atmospheric variability. *J. Climate*, **2**, 1447–1462.

Dey, B. and O.S.R.U. Bhanu Kumar, 1983: Himalayan winter snow cover area and summer monsoon rainfall over India. *J. Geophys. Res.*, **88**, 5471–5474.

Dickson, R.R., 1984: Eurasian snow cover versus Indian monsoon rainfall—An extension of the Hahn-Shukla results. *J. Clim. Appl. Meteor.*, **23**, 171–173.

Hahn, D.J. and J. Shukla, 1976: An apparent relationship between Eurasian snow cover and Indian monsoon rainfall. *J. Atmos. Sci.*, **33**, 2461–2462.

Hoskins, B.J. and D.J. Karoly, 1981: The steady linear response on a spherical atmosphere to thermal and orographic forcing. *J. Atmos. Sci.*, **38**, 1179–1196.

Iwasaki, T., 1991: Year-to-year variation of snow cover area in the Northern Hemisphere. *J. Meteor. Soc. Japan*, **69**, 209–217.

Jaeger, L., 1976: *Monatskarten des Niederschlags für die ganzeErde.* Berichte Deutsches Wetterdienstes, Nr. 139, Offenbach, 38 pp.

Kang, I.-S., 1990: Influence of zonal mean flow change on stationary wave fluctuations. *J. Atmos. Sci.*, **47**, 141–147.

Kitoh, A. and T. Tokioka, 1986: A simulation of the tropospheric general circulation with the MRI atmospheric general circulation model. Part II: The July performance. *Pap. Meteor. Geophys.*, **37**, 145–168.

Kitoh, A., K. Yamazaki and T. Tokioka, 1988: Influence of soil moisture and surface albedo changes over the African tropical rain forest on summer climate investigated with the MRI·GCM-I. *J. Meteor. Soc. Japan*, **66**, 65–86.

Kodera, K. and M. Chiba, 1989: Western Siberian spring snow cover and east Asian June 500 mb hieght. *Papers Meteor. Geophys.*, **40**, 51–54.

Kuhle, M., 1987: Subtropical mountain- and highland-glaciation as Ice Age triggers and the waning of the glacial period in the Pleistocene. *GeoJournal*, **14.4**, 393–421.

Lamb, H.H., 1977: *Climate. Present, past and future. Vol. 2 Climatic history and future.* 835 pp. William Clowers & Sons, Ltd., Beccles.

Legetes, D.R., 1987: A climatology of global precipitation. *Publications in Climatology*, **40-1**, 85 pp.

Manabe, S. and D.G. Hahn, 1977: Simulation of tropical climate of an Ice Age. *J. Geophys. Res.*, **82**, 3889–3911.

Matthews, E., 1983: Global vegetation and land use: new high resolution data bases for climate studies. *J. Clim. Appl. Meteor.*, **22**, 474–487.

Miyakoda, K. and J.-P. Chao, 1982: Essay on dynamical long-range forecasting of atmospheric circulation. *J. Meteor. Soc. Japan*, **60**, 292–308.

Morinaga, Y., 1987: Interaction between snow cover and atmospheric circulation in the Northern Hemisphere. Master thesis, Institute of Geoscience, University of Tsukuba, 55 pp.

Morinaga, Y. and T. Yasunari, 1987: Interactions between the snow cover and the atmospheric circulations in the northern hemisphere. *IAHS Publications* No. 166, 73–78.

Morinaga, Y. and H. Igarashi, 1991: Relationships between snow cover extent and snow mass derived from Nimbus-7 SMMR data over the Eurasian continent. *Climatological Notes*, Univ. of Tsukuba, No. 40, 101–110.

Oglesby, R.J., 1990: Sensitivity of glaciatin to initial snow cover, CO2, snow albedo, and oceanic roughness in the NCAR CCM. *Climate Dynamics*, **4**, 219–235.

Posey, J.W. and P.F. Clapp, 1964: Global distribution of normal surface albedo. *Geofis. Int.*, **4**, 33–48.

Prell, W.L. and J.E. Kutzbach, 1988: Monsoon variability over the past 150,000 years. *J. Geophys. Res.*, **92**, D7, 8411–8425.

Schutz, C. and L.B. Bregman, 1987: Global annual snow accumulation by months. RAND Note N-2551-AS.

Short, D.A., J.G. Mengel, T.J. Crowly, W.T. Hide and G.R. North, 1991: Filtering of Milankovitch cycles by earth's geography. *Quaternary. Res.*, **35**, 157–173.

Smagorinsky, J., 1953: The dynamical influence of large-scale heat sources and sinks on the quasi-stationary mean motions of the atmosphere. *Quart. J. Roy. Meteor. Soc.*, **79**, 342–366.

Tokioka, T., K. Yamazaki, I. Yagai and A. Kitoh, 1984: A description of the Meteorological Research Institute atmospheric general circulation model (The MRI·GCM-I). *Tech. Rep. of the MRI.* No. 13. 249 pp.

Webster, P., 1982: Seasonality in the local and remote atmospheric response to sea surface temperature anomalies. *J. Atmos. Sci.*, **39**, 41–52.

Williams, J., 1975: The influence of snowcover on the atmospheric circulation and its role in climatic change: A analysis based on results from the NCAR global circulation model. *J. Appl. Meteor.*, **14**, 137–152.

Yamazaki, K., 1989: A study of the impact of soil moisture and surface albedo changes on global climate using the MRI·GCM-I. *J. Meteor. Soc. Japan*, **67**, 123–146.

Yasunari, T., 1987: Global structure of the El Niño/Southern Oscillation. Part II. Time evolution. *J. Meteor. Soc. Japan*, **65**, 81–102.

Yasunari, T., 1988: Global teleconnections associated with Indian monsoon and the ENSO. *Meteor. Res. Report, Univ. of Tokyo*, **88-1**, 30–38.

Yasunari, T., 1990: Impact of Indian monsoon on the coupled atmosphere/ocean system in the tropical Pacific. *Meteor. & Atmos. Phys.*, **44**, 29–41.
Yasunari, T., 1991: Monsoon and ENSO: A coupled ocean/land/atmosphere system. *TOGA Notes*, No. 2, 9–13.
Yeh, T.C., R.T. Wetherald and S. Manabe, 1983: A model study of the short-term climatic and hydrologic effects of sudden snow cover removal. *Mon. Wea. Rev.*, **111**, 1013–1024.
Yeh, T.C., R.T. Wetherald and S. Manabe, 1984: The effect of soil moisture on the short-term climate and hydrology change—A numerical experiment. *Mon. Wea. Rev.*, **112**, 474–490.

ユーラシア大陸の積雪が北半球暖候季の大気に与える影響について
—MRI·GCM による数値実験—

安成哲三
（筑波大学地球科学系）
鬼頭昭雄・時岡達志
（気象研究所気候研究部）

ユーラシア大陸の冬の終わりの積雪が、北半球の引き続く暖候季（春・夏）の大気状態にどのような影響を及ぼすかを、気象研究所の大気大循環モデルを用いた数値実験により調べた。

三月初めにユーラシア大陸の積雪域に 5 cm（水当量）の積雪を上乗せしたラン (SNOW run) を夏の終わりまで積分して、コントロール・ラン (CNTL run) と比較することにより、正の積雪偏差が春から夏にかけての大気状態をどのように変えるかを評価した結果、以下のことが明かとなった。

(1) 春には、アルベード効果が、比較的低緯度で日射の強いチベット高原付近を中心に顕著に現れ、顕・潜熱フラックスの減少、地上気温の低下、大気全加熱量の減少をもたらす。

(2) 一方夏には、より高緯度側の中央アジア・東アジアの平原を中心に、融雪水文学的過程による土壌水分量の増加と地上気温の低下が卓越する。しかしながら、蒸発量の増大は、積雲対流を活発化させることにより、地表付近での顕熱フラックスの減少による大気全加熱量の減少を、部分的に補償する役割を果している。この蒸発・対流フィードバックは、しかし、地表面のより湿った（低温の）状態を夏の間を通して持続させる働きもしている。アジアモンスーンは、全体として弱まっている。

(3) これらの地域での大気の（相対的の）冷源は、局地的な大気循環の偏差を作り出すだけではなく、定常ロスビー波の伝播により、春・夏を通じて北太平洋から北米大陸上に、顕著なテレコネクション・パターンを形成する。この循環パターンにより、北米大陸部は低気圧性循環が卓越し、暖候季を通じて低温傾向が維持される。

これらの結果が、氷期論に与える示唆についても、簡単な議論を加えた。